Ionospheric Response to the St. Patrick's Day Space Weather Events in March 2012, 2013, and 2015 at Southern Low and Middle Latitudes

Sushil Kumar[1] [iD] **and Vickal V. Kumar[2]**

[1]School of Engineering and Physics, The University of the South Pacific, Suva, Fiji, [2]Space Weather Services, Australian Bureau of Meteorology, New South Wales, Australia

Abstract The changes in critical frequency of the F_2 layer (f_oF_2) and f_oF_2 deviation (Δf_oF_2) have been determined for three geomagnetic storms in March of the years 2012, 2013, and 2015 at low-latitude stations, Darwin (geomag. lat. 21.96°S) and Townsville (28.95°S), and midlatitude stations, Brisbane (36.73°S), Canberra (45.65°S), and Hobart (54.17°S). The moderate storm during 15–16 March 2012 ($Dst = -87$ nT) showed a decrease in f_oF_2 at midlatitude and no effect at low-latitude stations. For the intense storm of 17–18 March 2013 ($Dst = -132$ nT) and the super storm of 17–18 March 2015 ($Dst = -222$ nT), some middle- to low-latitude stations showed a short-duration increase in f_oF_2, but all stations showed a long-duration decrease in f_oF_2 during the recovery phases with $\Delta f_oF_2\%$ varying from 26% (Darwin) to 36.6% at Hobart for the March 2013 storm and above 40% for the March 2015 storm at all of the stations. Short-duration (~2–4 hr) increase in f_oF_2 seems to be associated with the prompt penetrating electric fields. Long-duration (>6 hr) decrease in f_oF_2 is mainly accounted to the decrease in thermospheric O/N_2 density ratio because of storm-induced high-latitude circulation of gas with depleted O/N_2 density ratio to lower latitudes and partly due to disturbance dynamo electric fields. A comparison of ionosonde given f_oF_2 for equinoctial storms (March 2013 and 2015) with similar strength Southern Hemisphere winter storms (July 2012 and June 2015) has been made with the IRI-2016 model f_oF_2 for Darwin, Brisbane, and Canberra stations.

1. Introduction

Geomagnetic storms are produced when the interplanetary magnetic field (IMF) B_Z component turns southward, strengthens (IMF $B_Z < -10$ nT), and remains southward for a substantial length of time (longer than ~3 hr; Gonzalez et al., 1994; Gonzalez & Tsurutani, 1987). Geomagnetic storms are an important space weather phenomenon that, apart from affecting ground and satellite-based technological and high-frequency communications systems, can severely affect the dynamics and structure of the Earth's entire thermosphere and ionosphere. The ionospheric response to a geomagnetic storm is called an ionospheric storm that describes the ionospheric variations due to geomagnetic disturbances. The ionospheric variations can be determined from the total electron content (TEC) or from the critical frequency of the F_2-layer (f_oF_2), which is a direct measure of the peak electron density (N_mF_2) of the F_2-region ionosphere. In general, F region ionization is positively correlated to the density ratio of atomic oxygen O and the molecular nitrogen N_2. The storm-time increase/decrease in f_oF_2/TEC is referred to as a positive/negative ionospheric storm (Astafyeva et al., 2015; Kumar, 2005, Mendillo, 2006; Titheridge & Buonsanto, 1988). Kumar and Parkinson (2017) using 50 years (1965–2015) of geomagnetic disturbance and f_oF_2 data from a worldwide network of 132 vertical incidence ionosondes have analyzed a global picture of ionospheric storms in N_mF_2. The high-latitude Joule heating (JH), which could persist for several days, is associated with auroral electric currents and generates storm-time thermospheric neutral winds with decreased O/N_2 density ratio and gravity waves, which can generate traveling atmospheric disturbances (TADs)/traveling ionospheric disturbances (TIDs; e.g., Balan et al., 2011; Habarulema et al., 2015). TADs/TIDs flow to middle and low latitudes, which, along with prompt penetration of electric fields (PPEFs; e.g., Huang et al., 2005) and disturbance dynamo electric fields (DDEFs; Blanc & Richmond, 1980; Fejer, 2011; Fejer et al., 1983; Scherliess & Fejer, 1997), mainly change the dynamics and composition of both the ionosphere and thermosphere globally, leading to the occurrence of positive/negative ionospheric storm. The PPEFs are associated with rapid changes in the magnetospheric convection electric fields and are well correlated with the IMF B_Z component,

whereas DDEFs are associated with the changes in the thermospheric neutral winds pattern. The PPEFs are instantaneous and of short duration (~1–2 hr) but under the long duration of IMF B_Z southward can last significantly long, up to 8–10 hr (Huang, 2008) and have the eastward/westward polarity on the day/nightside. The DDEFs come with timescales from a few to several hours but last longer and change slowly. They can affect the low-latitude ionosphere up to a day or two after the onset of the storm and dominate during the recovery phase of the storm. The changes in the neutral composition due to storm-time thermospheric neutral winds with a decreased O/N_2 density ratio is mainly responsible for low- and middle-latitude negative ionospheric effects at the nighttime and during the recovery phase of the storms. However, the relative contribution of storm-time electrodynamical and compositional changes in the ionosphere varies with location, season, local time, storm phase and its intensity, and other factors (Liu et al., 2014).

Three geomagnetic storms with moderate, intense, and very intense (severe) magnitude occurred near the St. Patrick's Day in March of years 2012, 2013, and 2015, respectively. These storms were driven by intense interplanetary coronal mass ejections. The variations in the interplanetary parameters obtained from the OMNI database associated with these three geomagnetic storms have been described by Verkhoglyadova et al. (2016). Lyons et al. (2016) presented observations of electric field modes and their ionospheric and magnetospheric effects associated with the March 2013 storm. They found a dramatic poleward expansion of the boundary of the auroral oval, strong auroral activity, and strong penetrating midlatitude convection and ionospheric currents. Also, the polar cap TEC enhancements moved into the auroral oval and subsequently moved equatorward. The St. Patrick Day geomagnetic storm of 17–19 March 2015 was the most intense storm of the current solar cycle 24 with a minimum Dst index of −222 nT. This storm is the most studied space weather event of solar cycle 24 with most articles published under JGR-Space Physics special collection on "Geospace system responses to the St. Patrick's Day storms in 2013 and 2015" (Zhang et al., 2017). Using multi-instrument (GPS receiver, Ionosonde, and Satellite) data, Astafyeva et al. (2015) analyzed the global ionospheric response of the March 2015 storm and found a complex effect varying with longitude and hemisphere, showing both positive and negative ionospheric storms in the TEC. Nava et al. (2016) analyzed the global and regional electron content data for the March 2015 storm at middle and low latitudes and found a positive ionospheric storm during the main phase of the storm and a long-lasting negative ionospheric storm during the recovery phase. Ray et al. (2017) analyzed the effect of the 17–18 March 2015 storm on TEC and amplitude and phase scintillations at five low-latitude GPS stations located around the 77°E longitude in the Indian sector and found a positive ionospheric effect in TEC on 17 March.

In this paper, we present a statistical analysis of the hourly value of f_oF_2 at two low- and three middle-latitude stations, in the Southern Hemisphere (Australian region) to determine the ionospheric effects of the three St. Patrick Day storms that occurred in the March month of years 2012, 2013, and 2015. The observed average sunspot numbers (R_Z) for the March month of the years 2012, 2013, and 2015 were 86.6, 78.3, and 54.5, respectively (http://www.sws.bom.gov.au/Solar/1/6). The latest version of the International Reference Ionosphere model called IRI-2016 has been used to obtain the f_oF_2 for two equinoctial storms (March 2013 and 2015) to compare with the ionosonde f_oF_2 observations at Darwin (DW), Brisbane (BR), and Canberra (CB) stations. For the details about the IRI-2016 model, the reader is referred to the recent paper by Bilitza et al. (2017). At these three stations (DW, BR, and CB), the ionosonde f_oF_2 data for the 17–18 March 2013 storm (min. $Dst = −132$ nT) have also been compared with the similar strength storm of 15–16 July 2012 (min. $Dst = −139$ nT) and for the 17–18 March 2015 storm (min. $Dst = −222$ nT) with the similar strength storm of 22–24 June 2015 storm (min. $Dst = −195$ nT). Monthly observed averaged R_Z for July 2012 and June 2015 were 84.5 and 72.1, respectively. The March and June geomagnetic storms in 2015 have been the first and second largest geomagnetic storms of the solar cycle 24. There have been several studies separately on the ionospheric effects of the March 2012, 2013, and 2015 storms (particularly of March 2015 storm), but there has been no study that compared their effects and with similar strength storms and with the ionospheric effects given by the IRI-2016 model.

2. Data and Analysis

The hourly values of f_oF_2 measured with the ionosonde at two low-latitude stations, DW (geomagnetic coordinates, 21.96°S, 202.84°E) and Townsville (TV; 28.95°S, 220.72°E), and three midlatitude stations, BR (36.73°S, 228.93°E), CB (45.65°S, 226.30°E), and Hobart (HO; 54.17°S, 226.52°E), were obtained from the
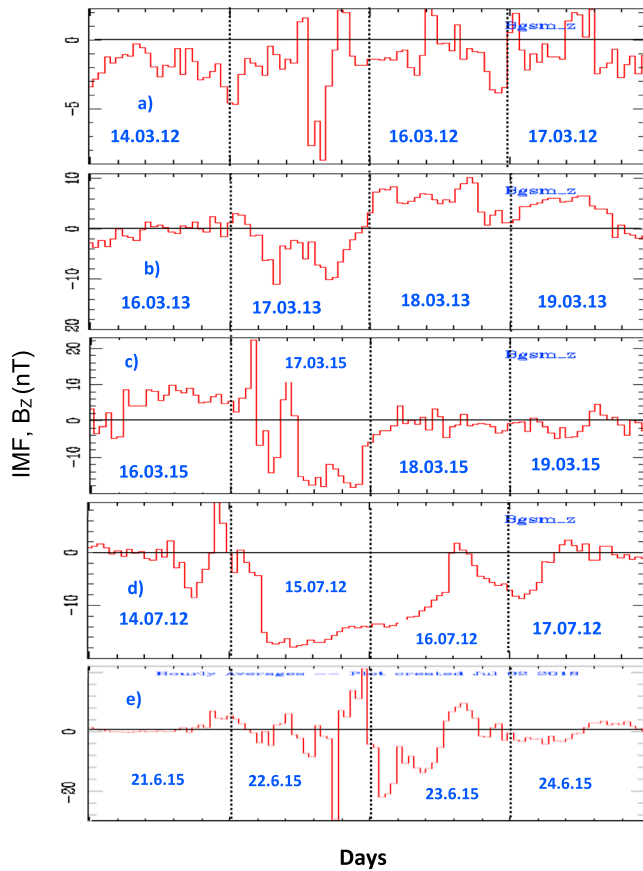
Figure 1. The temporal variation of interplanetary magnetic field (IMF) B_Z component (GSM coordinates) from the OMNI database (ACE magnetometer): (a) 14–17 March 2012, (b) 16–19 March 2013, (c) 16–19 March 2015, (d) 14–17 July 2012, and (e) 21–25 June 2015.

World Data Centre, Bureau of Meteorology, Australia (online at http://www.sws.bom.gov.au/World_Data_Centre). The f_oF_2 values are scaled to the nearest 0.1 MHz (Kumar & Parkinson, 2017). The local time of stations is given as follows: LT (DW) = UT + 8.7 hr, LT (TV) = UT + 9.8 hr, LT (BR) = UT + 10.2 hr, LT (CB) = UT + 9.9 hr, and LT (HO) = UT + 9.8 hr. The values of f_oF_2 extracted online are scaled up by a factor of 10, and the same values have been used in our analysis. The f_oF_2 is also used to calculate N_mF_2 of the F_2 region ionosphere using a simple relationship, $N_mF_2(cm^3) = 1.24 \times 10^4 \times f_oF_2^2$, where f_oF_2 is in megahertz (Kumar & Parkinson, 2017). The stations within geomagnetic latitude 10–30°S are considered as low-latitude stations and stations within 30–60°S as midlatitude stations. The monthly median values for 24 hr of the day (0–23 h) were calculated excluding the five most disturbed days of the respective month, and then the percentage deviation of storm-time f_oF_2 values from the median values were determined to see the amount of storm-time change in the f_oF_2. The *Dst* index values were obtained from the World Data the Centre, Kyoto University, Kyoto, Japan (online at http://wdc.kugi.kyoto-u.ac.jp/). The plots of IMF B_Z component variation for these (March 2012, 13, 15, July 2012, and June 215) storms obtained from the ACE Science Center, web http://www.srl.caltech, are shown in Figure 1. Thermospheric O/N_2 density data as measured by the Global Ultraviolet Imager (GUVI) on board the Thermosphere, Ionosphere, Mesosphere Energetics, and Dynamics (TIMED) satellite were obtained from http://guvitimed.jhuapl.edu/. The IRI-2016 model was run online https://omniweb.gsfc.nasa.gov/vitmo/IRI-2016_vitmo.html to obtain the modeled storm-time f_oF_2 values keeping the F peak storm model on using F peak electron density model, URSI, and F peak height model, AMTB2013, and the f_oE storm model was kept off. The percentage changes in f_oF_2 ($\Delta f_oF_2\%$) from median values during the storms were calculated using the following:

$$\Delta f_oF_2\% = \frac{f_oF_{2\text{storm}} - f_oF_{2\text{mean}}}{f_oF_{2\text{mean}}} \times 100 \qquad (1)$$

3. Results

3.1. f_oF_2 Perturbations During the St. Patrick Day Storms in March 2012, 2013, and 2015

3.1.1. The St. Patrick's Day Storm of March 2012

The interplanetary parameters for 15–18 March 2012 have been described by Tsurutani et al. (2014) and Verkhoglyadova et al. (2016). This geomagnetic storm was associated with the southward turning of IMF $B_Z < -5$ nT (Figure 1a) and in the post interplanetary shock (Tsurutani et al., 2014). It was caused by sheath fields behind the strong interplanetary fast forward shock and the magnetic cloud (MC) with low-plasma β of 0.01 that occurred during 21:35 UT on 15 March to 10:50 UT on 16 March. The main phase onset of this moderate storm started at 13 UT on 15 March with a minimum *Dst* = −87 nT at 20 UT. The *AE* index increased to a maximum of 1,154 nT at 18 UT on 15 March. Figure 2a shows variation of *Dst* and *AE* indices from 14 to 17 March 2012, monthly median f_oF_2 values (black solid line) for March 2012 excluding five most geomagnetically disturbed days with ±1 standard deviation (σ; dashed lines) and the storm-time f_oF_2 (red markers) from 14 to 17 March 2012 at BR (Figure 2b), CB (Figure 2c), and HO (Figure 2d) stations. A night-time decrease in f_oF_2 started during the main phase onset of this storm at BR (geomag. lat. 36.73°S) and CB (geomag. lat. 45.65°S) stations between 14 and 15 UT on 15 March (~00–01 LT, 16 March) and lasted until ~08 UT (~18 LT) on 16 March at BR and until ~20 UT at CB and HO stations on 16 March (~06 LT, 17 March). The decrease in f_oF_2 was comparatively more and of longer duration at CB as compared to BR and HO stations. At HO station, there was no f_oF_2 data available during 11–22 UT on 15 March. The percentage decrease in f_oF_2 from monthly median values ($\Delta f_oF_2\%$), calculated using equation (1), was mostly
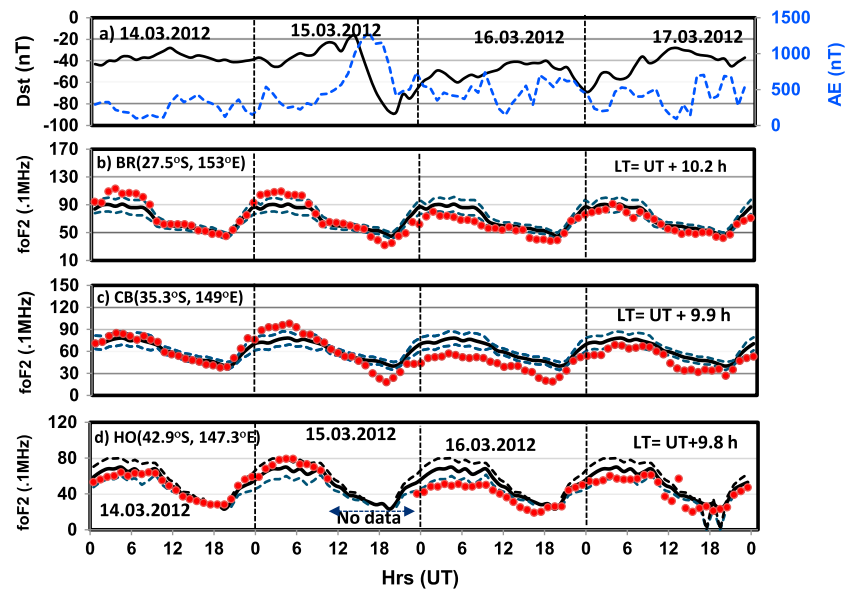
Figure 2. (a) Variation of *Dst* (solid line) and *AE* (dashed line) indices during 14–17 March 2012. Variation of monthly median f_oF_2 (MHz × 10^{-1}) values (black solid line) for March 2012 excluding the five most geomagnetically disturbed days with $\pm 1\sigma$ lines (dashed gray color lines) and current f_oF_2 (red markers) during 14–17 March 2012 at Brisbane (BR) (b), Canberra (CB) (c), and Hobart (HO) (d) stations.

less than 25% at BR and mostly larger than 25% at CB, which at times went up to 50–56%. There was no noticeable change in the f_oF_2 over 1 standard deviation (σ) values from the median at DW (geomag. lat. 21.96°S) and TV (geomag. lat. 28.95°S) stations, not shown in Figure 2, indicating that this storm affected the ionosphere only up to midlatitudes in the Southern Hemisphere. Looking at f_oF_2 variation before and after the storm around $\pm 1\sigma$, this has been taken into account for the day-to-day variability of the ionosphere (Prasad et al., 2016). However, higher value of σ (e.g., $\pm 2\sigma$) can be also taken for higher confidence (95%) due to several factors such as gravity waves, planetary waves, tides, and so on apart from space weather phenomena. The average Δf_oF_2% (equation (1)) and the duration of storm effect are shown in Table 1, which indicate that the amount of decrease in f_oF_2 and the duration of decrease were more at CB as compared to BR. During the recovery phase of this storm, there occurred one more moderate storm starting at ~20 UT on 16 March with *Dst* ~ −69 nT at 00 UT on 17 March, associated with that a slight decrease in f_oF_2 can be seen at CB and HO stations (Figure 2).

3.1.2. The St. Patrick's Day Storm of March 2013

The interplanetary parameters for this storm during 17–20 March 2013 have been presented by Verkhoglyadova et al. (2016) and Lyons et al. (2016). This St. Patrick Day storm was associated with the coronal mass ejections that resulted in a shock that impacted the magnetosphere at 06 UT on 18 March (Baker

Table 1
The Geographic and Geomagnetic Coordinates of IPS Stations and Average Percentage of Change in Ionosonde Given f_oF_2, Δf_oF_2%, and Duration of Change in f_oF_2, Δf_oF_2 (hr), From the Median Values During Three Storms Near St. Patrick's Day in Years 2012, 2013, and 2015

Station	Geographic. coordinates lat (°S), long (°E)	Geomagnetic coordinates GLat (°S), GLong (°E)	March 2012 −88 nT		March 2013 −132 nT		March 2015 −222 nT	
			Δf_oF_2 (%)	Δf_oF_2 (hr)	Δf_oF_2 (%)	Δf_oF_2 (hr)	Δf_oF_2 (%)	Δf_oF_2 (hr)
Darwin (low latitude)	12.45, 130.95	21.96, 202.84	NC	NC	−26.0	18	−42.3	24
Townsville (low latitude)	19.63, 146.85	28.95, 220.72	NC	NC	−29.9	15	ND	ND
Brisbane (midlatitude)	27.53, 152.92	36.73, 228.93	−20.9	16	−29.1	21	−44.8	26
Canberra (midlatitude)	35.32, 149.00	45.65, 226.30	−29.6	39	−30.0	26	−46.5	20
Hobart (midlatitude)	42.92, 147.32	54.17, 226.52	ND	ND	−36.6	36	−34.7	23

Note. NC indicates no change, and ND indicates no good data. The minus sign in Δf_oF_2% indicates the decrease in f_oF_2 from median level.
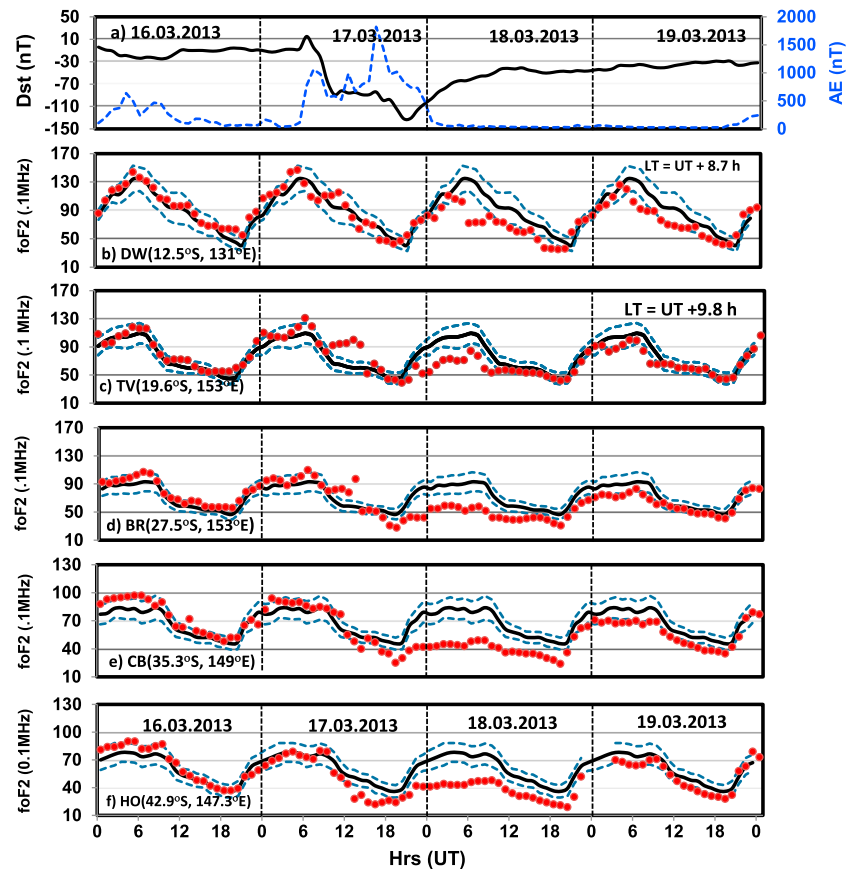
Figure 3. (a) Variation of *Dst* (solid line) and *AE* (dashed line) indices during 16–19 March 2013. Variation of monthly median f_oF_2 (MHz × 10^{-1}) values (black solid line) for March 2013 excluding the five most geomagnetically disturbed days with ±1σ lines (dashed gray color lines) and current f_oF_2 (red markers) during 16–19 March 2013 at Darwin (DW) (b), Townsville (TV) (c), Brisbane (BR) (d), Canberra (CB) (e), and Hobart (HO) (f) stations.

et al., 2014). The IMF B_Z variation during 16–19 March 2013 is shown in Figure 1b. The storm developed through a two-step growth in the ring current in which the first step of the decrease in the *Dst* occurred coincident with the initial southward turning of IMF B_Z in the sheath region and *Dst* reached to a minimum value of −89 nT at 10 UT on 17 March. During the slow recovery of the first step of the storm (*Dst*), a long-duration MC occurred at ~15:22 UT on 17 March to ~16:48 UT on 19 March (Verkhoglyadova et al., 2016), and during this MC the IMF *Bz* turned southward and the second step storm development started in which *Dst* went to a minimum of −132 nT at 20 UT and *AE* index to a maximum of 1,822 nT at 16 UT on 17 March (Figure 3a). The f_oF_2 measurements from the Space Weather Services (SWS), Australia, at ground ionosonde stations (http://www.sws.bom.gov.au/World_Data_Centre) DW (Figure 3b), TV (Figure 3c), BR (Figure 3d), CB (Figure 3e), and HO (Figure 3f) stations are shown in Figure 3 with the format of the data same as in Figure 2. An increase in f_oF_2 from the median level that began toward the end of the first step storm development occurred between 10 and 14 UT (~20–24 LT, premidnight) on 17 March, which can be clearly seen at TV and BR stations, but no change in f_oF_2 occurred at DW. During this time, TV station showed an increase in f_oF_2 varying between 38.4–66.7% estimated using equation (1). The second step of the storm development started from about 15 UT to a minimum of *Dst* = −132 nT at 20 UT on 17 March associated with which a decrease in f_oF_2 started promptly with the first start at HO at ~13 UT (~23 LT) and then progressed toward TV station where a decrease in f_oF_2 started at around 19 hr (~05 LT, 18 March). However, at DW a delayed decrease in f_oF_2 started during the recovery phase of this storm at ~04 UT (~13 LT) on 18 March. The amount and duration of f_oF_2 decrease were larger at HO and CB stations as compared to BR and TV stations and were minimum at DW as can be seen from Figure 3. Another important feature to note is the strong decrease in f_oF_2 (negative ionospheric effect) in the local daytime (~20–08
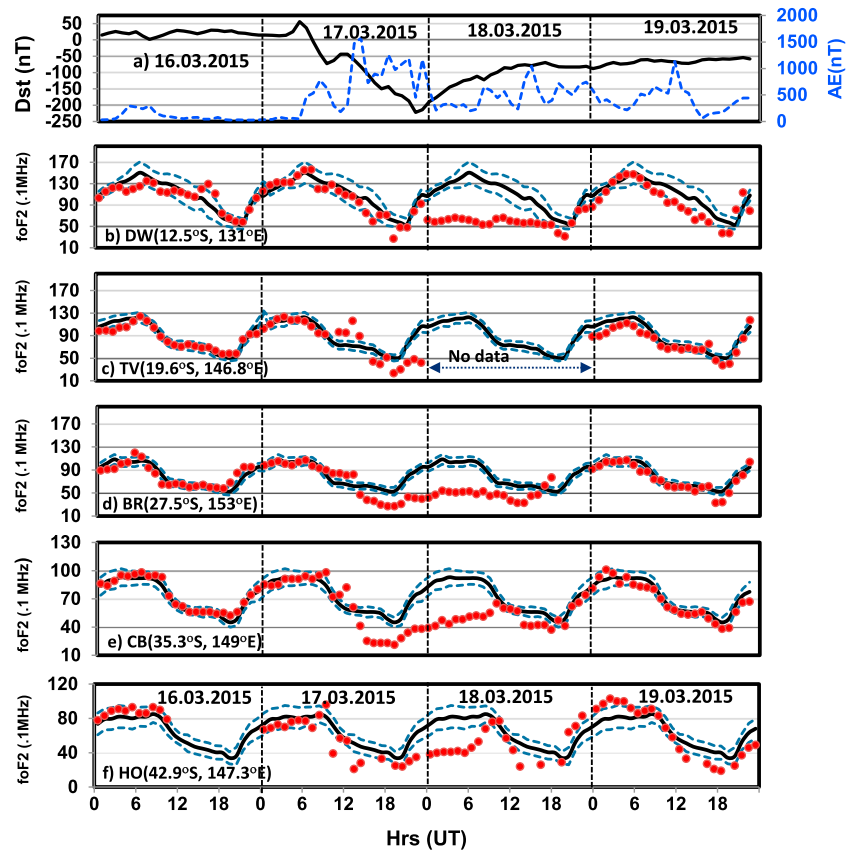
Figure 4. (a) Variation *Dst* (solid line) and *AE* (dashed line) indices during 16–19 March 2015. Variation of monthly median f_oF_2 (MHz $\times$ 10^{-1}) values (black solid line) for March 2015 excluding the five most geomagnetically disturbed days with $\pm 1\sigma$ lines (dashed gray color lines) and current f_oF_2 variations (red markers) during 16–19 March 2015 at Darwin (DW) (b), Townsville (TV) (c), Brisbane (BR) (d), Canberra (CB) (e), and Hobart (HO) (f) stations.

UT) as compared to that at the local nighttime (08–20 UT). The percentage decrease in f_oF_2 (Δf_oF_2%) using equation (1) varied between ~15% and 46% at DW, 15% and 40% at TV, 20% and 50% at BR, 20% and 48% at CB, and 18% and 51% at HO with average percentage decrease in f_oF_2 above 26% (Table 1) at all the stations except at TV where data were not available. The quantitative estimate of average percentage decrease in f_oF_2 (equation (1)) for the duration of the decrease below 1σ estimated from Figure 3 has been summarized in Table 1, which shows the highest value of Δf_oF_2% of 36.6% at HO that subsequently reduced toward lower-latitude stations to a minimum of 26% at DW. The duration of decrease in f_oF_2 (Table 1) counted from the decrease below 1σ from a median value to recovery to the same level shows a maximum duration of decrease of 36 hr at HO and about 50 hr at CB, 40 hr at BR, and minimum of 15 and 18 hr at TV and DW stations, respectively.

3.1.3. The St. Patrick's Day Storm of March 2015

The interplanetary parameters and solar wind conditions associated with the 17–18 March 2015 storm have been presented by several researchers (e.g., Alberti et al., 2017; Guerrero et al., 2017; Marubashi et al., 2016; Verkhoglyadova et al., 2016; Wu et al., 2016). The IMF B_Z variation during 16–19 March 2015 (Figure 1c) shows two southward turnings of IMF B_Z with the second one strong (< -15 nT) and of longer duration ($>$10 hr). This storm of 17–18 March 2015 with a minimum *Dst* index of -222 nT developed through a two-step development in the ring current as shown in Figure 4a. The first step was caused by a southward IMF B_Z in the sheath region and the second step by the passage of a MC (Wu et al., 2016), thus showing sheath-sheath-ejecta scenario for the multistep development of this superstorm. The second step of the storm development was of longer duration that was consistent with an intense (-10 to -20 nT) and long
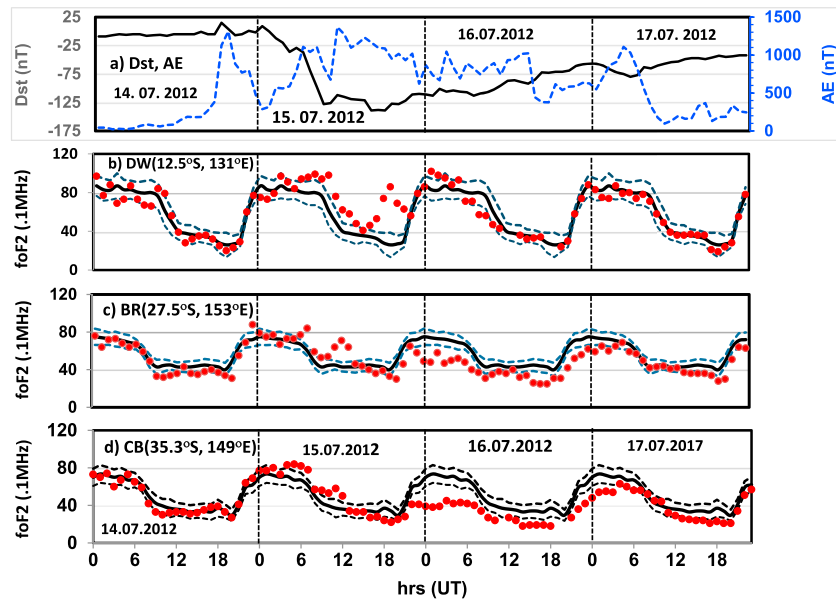
Figure 5. (a) Variation of *Dst* (solid line) and *AE* (dashed line) indices during 14–17 July 2012. Variation of monthly median f_oF_2 (MHz × 10^{-1}) values (black solid line) for July 2012 excluding the five most geomagnetically disturbed days with $\pm 1\sigma$ lines (dashed gray color lines) and current f_oF_2 variations (red markers) during 14–17 July 2012 at Darwin (DW) (b), Brisbane (BR) (d), and Canberra (CB) (d) stations.

duration of southward IMF B_Z in the MC that intensified the storm. The *AE* index reached to a maximum of 778 nT at 08 UT on 17 March during the first step development of the storm, then decreased to 187 nT at 11 UT, and then sharply increased to 1,570 nT at 14 UT and remained higher for about 9 hr (Figure 4a). The f_oF_2 variation as given in Figures 4b–4f did not show any noticeable change at any station from the median level $\pm 1\sigma$ during the first-step development of the storm to −73 nT until 09 UT on 17 March 2015. During the second step development of the storm, there occurred a short duration increase in f_oF_2 for about 2–4 hr during 10–14 UT (~20–00 LT, premidnight) at all the stations except at DW. During the latter part of the second step development of this storm between 17 and 22 UT and its recovery phase, a substantial decrease in f_oF_2 for longer duration occurred at all the stations. The decrease first started at HO (Figure 4f) and CB (Figure 4e) stations and subsequently at other lower-latitude stations. However, at DW (Figure 4b), a decrease in f_oF_2 started during the recovery phase of the storm with no decrease during the second step of the storm development. Similar to the March 2013 storm, this storm also showed a strong decrease in f_oF_2 (negative ionospheric effect) in the local daytime (~20–08 UT) as compared to that in the local nighttime (08–20 UT). At TV (Figure 4c) station on 18 March and for a few hours at BR (Figure 4d) station during the recovery phase, f_oF_2 data are not available due to technical problems. The percentage decrease in f_oF_2 ($\Delta f_oF_2\%$) calculated using equation (1) varied between 35–60% at DW, 40–58% at BR, 43–54% at CB, and 35–50% at HO with average percentage decrease in f_oF_2 above 34% (Table 1) at all the stations except at TV where data were not available. The quantitative estimate of the average percentage decrease in f_oF_2 for the duration of the decrease below 1σ summarized in Table 1 shows that the $\Delta f_oF_2\%$ varied between 42.3% and 46.5% with 20–26 hr duration.

3.2. Comparison of the March 2013 and 2015 Storm Effects With the Two Similar Strength Storms Using Ionosonde Data: The July 2012 and June 2015

There occurred an intense storm on 15 July 2012 that developed in two steps with the first step (main phase onset) commencing at about 06:40 UT and giving a minimum *Dst* index of −128 nT at ~09 UT on 15 July. As shown in Figure 5a, the second step of the ring current development occurred during the recovery of the first step storm development and produced a minimum *Dst* index of −139 nT at ~16 UT on 15 July. This storm was also associated with high *AE* values particularly during the second step that extended well into the recovery phase until 15 UT on 16 July (Figure 4a). This storm was unique in the sense that the IMF B_Z

Table 2

A Comparison of Average Δf_oF_2 (%) and Δf_oF_2 (hr) Using Ionosonde f_oF_2 Between March 2013 and July 2012 Storms at Three Stations During Recovery Phases of These storms

Station	March 2013 −132 nT		July 2012 −139 nT	
	Δf_oF_2 (%)	Δf_oF_2 (hr)	Δf_oF_2 (%)	Δf_oF_2 (hr)
Darwin (low latitude)	−26.0	18	NC	NC
Brisbane (midlatitude)	−29.1	21	−24.8	24
Canberra (midlatitude)	−30.0	26	−28.6	29

Note. NC indicates no change. The minus sign in Δf_oF_2% indicates the decrease in f_oF_2 from median level.

was southward below −10 nT for a long duration of about 31 hr from ~08 hr UT on 15 July to 15 UT on 16 July (Figure 1d; Liu et al., 2014). In terms of the storm strength given by the *Dst* index, this storm is comparable to the 17–18 March 2013 storm that had a minimum *Dst* value of −132 nT. The effect of 15–16 July 2012 storm on f_oF_2 has been compared with the effect of 17–18 March 2013 storm at a low-latitude station, DW, and two midlatitude stations, BR and CB. Figures 5b–5d show the variation of f_oF_2 at these stations on 15–16 July 2012. There was an increase in f_oF_2 during both the step developments of July 2012 storm that was most (up to 210%) pronounced at the low-latitude station, DW (Figure 5b), less (~48%) at BR (Figure 5c), and least (24%) at CB (Figure 5d) and lasted for about 6, 3, and 3 hr, respectively. During the recovery phase of the July 2012 storm, there occurred a long-duration decrease in the f_oF_2 at midlatitude stations BR and CB only, which has been compared with a decrease in f_oF_2 during the recovery phase of the March 2013 storm in Table 2. Table 2 shows that at BR and CB stations, the decrease in f_oF_2 during the March 2013 storm was slightly larger but of lesser duration as compared to the July 2012 storm. During the recovery phase, the DW station showed no effect for the July 2012 storm but showed a long-duration (18 hr) negative (decrease) effect in f_oF_2 for the March 2013 storm. However, during the main phase onset of both the storms, a low-latitude station, DW, showed no change in f_oF_2 for the March 2013 storm (Figure 3b) and intense and positive effect for the July 2012 storm (Figure 5b).

The intense storm of 22–24 June 2015 was the second largest geomagnetic storm of the solar cycle 24, after the St. Patrick's Day storm of 17–18 March 2015. Two coronal mass ejections that hit the Earth on 22 June at 05:45 UT and at 18:30 UT, respectively, produced this storm (Astafyeva et al., 2016). As shown in Figure 1e, the IMF B_Z sharply turned southward to < −20 nT with a minimum value of −37 nT at ~19 UT (Astafyeva et al., 2016) on 22 June corresponding to which the first step of the ring current development occurred giving a *Dst* index of −112 nT at 20 UT on 22 June. The second southward turning of IMF *Bz* started at ~02 UT on 23 June (Figure 1e) and remained mostly negative between −10 and −20 nT until ~10 UT and produced a second significant decrease in *Dst* index to a minimum value of −195 nT at ~ 5:00 UT on 23 June (Figure 6a). As shown in Figure 6a, the *AE* index increased during the period 07 UT on 22 June to 13 UT on 23 June with a maximum value of 1,636 nT at 18 UT on 22 June. The variation of interplanetary parameters of this storm shows that its multistep development is consistent with sheath-sheath-ejecta scenario (https://arxiv.org/pdf/1508.01267.pdf). The variation in f_oF_2 for this storm on 21–25 June 2015 at three stations is shown in Figures 6a–6d. Associated with the first step development of this storm, there occurred no change in f_oF_2 at all three stations, and associated with the second step storm development, the f_oF_2 increased sharply with a maximum increase at the low-latitude station DW (Figure 6b). This increase in f_oF_2 lasted for about 3–5 hr with a few hours in the recovery phase. The percentage increase in f_oF_2 (Δf_oF_2%) calculated using equation (1) varied from about 25% to 61% at DW, 19.7% to 39% at BR, and 28.9% to 38.9% at CB. However, for the March 2015 storm, f_oF_2 decreased strongly (~42–47%) for a long duration, and the decrease started during the second step storm development and lasted well into the recovery phase. A comparison of the average change in f_oF_2 during the recovery phase of both the storms shown in Table 3 gives very contrasting effects of these storms in f_oF_2 both at low- and middle-latitude stations where the March 2015 storm showed a strong long-duration negative ionospheric effect and the June storm showed a short-duration strong positive ionospheric effect.

3.3. Comparison Between Ionospheric Effect Shown by the IRI-2016 and the Ionosonde f_oF_2
3.3.1. The St. Patrick Day Storms: March 2013 and 2015

The latest version of the IRI-2016 model has been used to obtain the hourly values of f_oF_2 that have been compared with those measured with an ionosonde for the intense March 2013 and the super intense March 2015 storms at a low-latitude station, DW, and two midlatitude stations, BR and CB. The observed average R_Z, 78.3 and 54.5, were used as solar activity parameter for the March 2013 and 2015, respectively. Figures 7a, 7b, and 7c show the variation of IRI-2016 f_oF_2 at these stations during 16–18 March 2013 with respect to the median values excluding five most disturbed days at three stations. There was a small increase in f_oF_2 between 00 and 08 hr on 16 March at three stations,
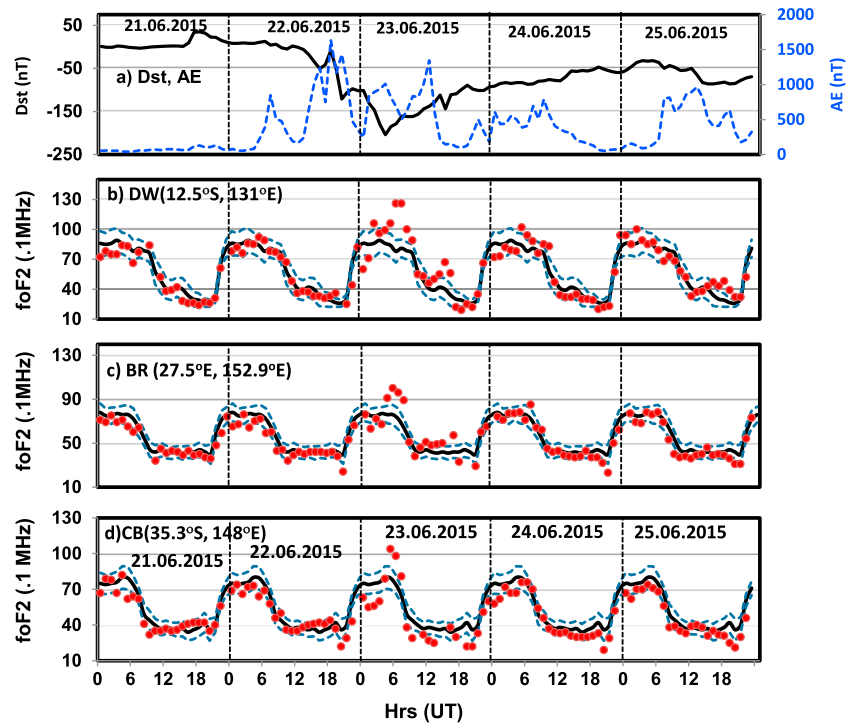
Figure 6. (a) Variation of *Dst* (solid line) and *AE* (dashed line) indices during 21–25 June 2015. Variation of monthly median f_oF_2 (MHz × 10^{-1}) values (black solid line) for June 2015 excluding the five most geomagnetically disturbed days with $\pm 1\sigma$ lines (dashed gray color lines) and current f_oF_2 variations (red markers) during 21–25 June 2015 at Darwin (DW) (b), Brisbane (BR) (d), and Canberra (CB) (d) stations.

which can be clearly seen at the CB station. An increase in f_oF_2 again began on 17 March at 00 UT and lasted until about 08 UT that can be clearly seen at CB. The f_oF_2 then started decreasing slowly and went below the normal time value at 09 UT at midlatitude stations CB and BR, whereas at the low-latitude station DW, f_oF_2 showed no decrease until about 12 UT. A decrease in f_oF_2 progressed from 09 UT and reached to its maximum value at 20 UT on 17 March at CW and at 11 UT on 18 March at BR. At DW station, a decrease in f_oF_2 progressed from 13 UT on 17 March and reached to its maximum value at 19 UT on 17 March. The maximum percentage decrease in f_oF_2 calculated using equation (1) (Δf_oF_2%) was 15.7%, 11.2%, and 9.2% at CB, BR, and DW stations, respectively. The amount and duration of the decrease in f_oF_2 were maximum at CB, less at BR, and least at DW showing a clear latitudinal dependence of the storm effect. Similarly, the variation in IRI-2016 given f_oF_2 at three same stations (one low-latitude and two midlatitude) during the storm of 17–18 March 2015 with respect to the median values excluding five most disturbed days is shown in Figures 8a, 8b, and 8c. A decrease in f_oF_2 first started at 09 UT on 17 March at CB and BR midlatitude stations, reached its maximum at around 10 UT on 18 March, and continued on 19 March. However, at low-latitude station DW, a decrease in f_oF_2 started at 12 UT on 17 March, reached its maximum at around 19 UT on 17 March, and then recovered to its normal value toward the end of 18 March. The maximum percentage decrease in f_oF_2 calculated using equation (1) (Δf_oF_2%) was 28.9%, 20.9%, and 9.2% at CB, BR, and DW stations, respectively.

The average values of Δf_oF_2% for the duration of decrease in f_oF_2 using IRI-2016 for March 2013 and March 2015 storms at three stations are summarized in Table 4. A comparison of results in Table 4 with those given in Table 1 for March 2013 storm shows that

Table 3
A Comparison of Average Δf_oF_2 (%) and Δf_oF_2 (hr) Using Ionosonde f_oF_2 Between March 2015 and June 2015 Storms at Three Stations During Their Recovery Phases of These Storms

	March 2015 −222 nT		June 2015 −195 nT	
Station	Δf_oF_2(%)	Δf_oF_2(h)	Δf_oF_2(%)	Δf_oF_2(h)
Darwin (low latitude)	−42.3	24	+30.1	06
Brisbane (midlatitude)	−44.8	26	+30.9	05
Canberra (midlatitude)	−46.5	20	+30.0	04

Note. The minus sign in Δf_oF_2% indicates the decrease in f_oF_2 from median level.
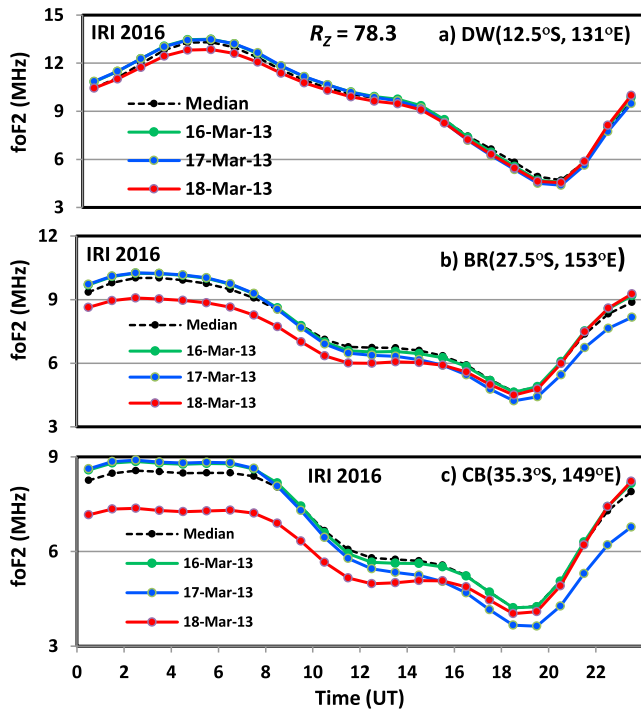
Figure 7. Change in IRI 2016 given f_oF_2 during 16–18 March 2013 with respect to March median values excluding the five most geomagnetically disturbed days at Darwin (DW) (a), Brisbane (BR) (b), and Canberra (CB) (c) stations.
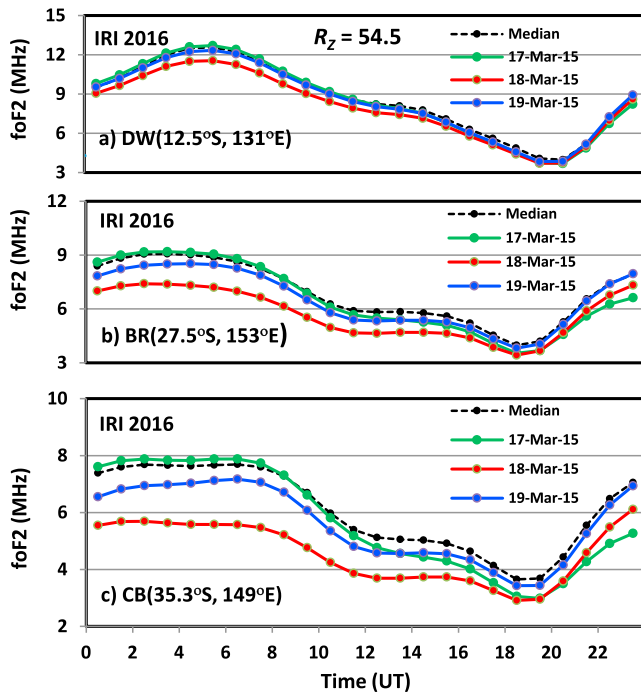

Figure 8. Change in IRI 2016 given f_oF_2 during 17–19 March 2015 with respect to March median values excluding the five most geomagnetically disturbed days at Darwin (DW) (a), Brisbane (BR) (b), and Canberra (CB) (c) stations.

$\Delta f_oF_2\%$ (equation (1)) using the IRI-2016 model is less by a factor of about 7, 4, and 3, at DW (low-latitude), BR (midlatitude), and CB (midlatitude) stations, respectively. A similar comparison of results in Table 4 with those given in Table 1 for the March 2015 storm shows that the IRI-2016 given $\Delta f_oF_2\%$ (equation (1)) is less by a factor of 6.7, 5, and 3, at DW (low-latitude), BR (midlatitude), and CB (midlatitude) stations, respectively. The duration of decrease in IRI-2016 f_oF_2 is longer by a factor of 1.4 (CB), 1.7 (BR), and 1.7 (DW) for March 2013 storm and by a factor of 3.2 (CB), 2.4 (BR), and 1.5 (DW) for the March 2015 storm than that observed by the ionosonde.

For the March 2013 storm, the maximum decrease in f_oF_2 occurred on 18 March for which the percentage decrease in f_oF_2 ($\Delta f_oF_2\%$) calculated using equation (1) has been compared for all three stations in Figure 9a. The percentage decrease in f_oF_2 ($\Delta f_oF_2\%$), in general, was within 2–5% at DW, 4–11% at BR, and 8–15% at CB stations. For the March 2015 storm also, the decrease in f_oF_2 was maximum on 18 March for which the percentage decrease in f_oF_2 ($\Delta f_oF_2\%$) calculated using equation (1) has been shown in Figure 9b for the three stations. The percentage decrease in f_oF_2 ($\Delta f_oF_2\%$), in general, was within 4–9% at DW, 9–20% at BR, and 15–28% at CB stations. At CB, the f_oF_2 showed almost the same trend as that at BR with about 8% more decrease during 0–11 UT and 6–7% afterward.

3.3.2. The July 2012 and June 2015 Storms

The 15–16 July 2012 and 22–24 June 2015 storms occurred during winter solstice of the Southern Hemisphere. To obtain f_oF_2 using the IRI-2016 model, the observed average R_Z, 84.5 and 72.1, were used as solar activity parameter for the July 2012 and the June 2015 storms, respectively. The July 2012 geomagnetic storm showed a strong increase in the ionosonde observed f_oF_2 with $\Delta f_oF_2\%$ (equation (1)) varying 24–210% for ~ 3–6 hr during the main phase onset on 15 July (Figures 5b, 5c, and 5d). The $\Delta f_oF_2\%$ calculated using equation (1) for IRI-2016 given f_oF_2 presented in Figure 10a for 15 July shows a week increase of 4–8% for a longer duration (~20 hr) at DW and BR stations, whereas the CB station showed further weaker increase of 2–3% for about 14 hr. On 16 July, the ionosonde observed f_oF_2 (Figures 5c and 5d) showed a long-duration (~10 hr) decrease of 30–60% at BR and CB stations. The $\Delta f_oF_2\%$ (equation (1)) using the IRI-2016 model shows an increase in f_oF_2 of about 7–10% at DW and 7–8% at BR, whereas the CB station shows a very weak decrease of 1–2% from 00 to 08 hr and then a similar increase from 18 to 23 UT (Figure 10b).

As presented in Figure 6, the ionosonde observed f_oF_2 for the June 2015 storm showed an increase of 20–61% for about 3–5 hr during the recovery phase on 23 June, but the IRI-2016 given f_oF_2 (Figure 10c) shows a long-duration (about a day) increase of about 8–10% at DW and 7% at BR, whereas the CW station shows a decrease of about 3–5%.

The average values of $\Delta f_oF2\%$ (equation (1)) and the duration of change in f_oF_2 using the IRI-2016 model for the July 2012 (15 and 16 July) and June 2015 (23 June) storms at three stations are summarized in Table 4. A comparison of results in Table 4 (IRI-2016) with Table 2 (ionosonde) for July 2012 storm shows very contrasting results. The IRI-2016 gives about 48 hr of increase in f_oF_2 with average $\Delta f_oF_2\%$ of about 7.8% at DW (low-latitude) and 6.7% at BR (midlatitude) stations, whereas ionosonde f_oF_2 shows no change in f_oF_2 at DW (low-latitude) station and a strong decrease in f_oF_2 with average $\Delta f_oF_2\%$ of about 24.8% at BR (midlatitude)

Table 4
The Δf_oF_2 (%) and Δf_oF_2 (hr) Using IRI-2016 Given f_oF_2 for March 2013 and March 2015 Storms and July 2012 (15–16 July) and June 2015 (23 June) Storms at Three Stations

Station	March 2013 −132 nT		March 2015 −222 nT		July 2012 −139 nT		June 2015 −195 nT	
	Δf_oF_2 (%)	Δf_oF_2 (hr)	Δf_oF_2 (%)	Δf_oF_2 (hr)	Δf_oF_2 (%)	Δf_oF_2 (hr)	Δf_oF_2 (%)	Δf_oF_2 (hr)
Darwin (low latitude)	−3.7	31	−6.3	35	+7.8	48	+9.4	24
Brisbane (midlatitude)	−7.4	35	−9.2	62	+6.7	48	+ 6.6	24
Canberra (midlatitude)	−10.5	37	−15.2	63	+2.8	15	−3.7	22

Note. The minus sign in Δf_oF_2% indicates the decrease in f_oF_2 from median level.

station. Interestingly, IRI-2016 for the CB station shows a weak increase in f_oF_2 for 15 hr with average Δf_oF_2% of about 2.8%, whereas the ionosonde showed a strong decrease in f_oF_2 with average Δf_oF_2% of about 28.6%. The IRI-2016 f_oF_2 results in Table 4 for the June 2015 storm show about 24 hr of the increase in f_oF_2 with an average Δf_oF2% of about 9.4% at DW (low-latitude) and 6.6% at BR (midlatitude), whereas the CB station shows a decrease in f_oF_2 for about 22 hr with an average Δf_oF_2% of about 3.7%. The ionosonde f_oF_2 for the June 2015 storm (Table 3) gives a strong increase in f_oF_2 with Δf_oF2% of about 30–31% at all three stations for a short duration of about 4–6 hr.

4. Discussion

The ionospheric response in f_oF_2, obtained from the ionosonde data, to the geomagnetic storms in March equinoctial month of years 2012, 2013, and 2015 has been analyzed at two low- and three middle-latitude stations in the Southern Hemisphere. The f_oF_2 changes using equation (1) during the intense storm of March 2013 have been compared with the similar strength southern winter storm of July 2012, and the f_oF_2 variations during the super intense storm of March 2015 have been compared with the similar strength winter storm of June 2015 at selected three stations. A comparison of ionosonde f_oF_2 for the March 2013 and 2015 storms has also been made with the f_oF_2 data obtained with the IRI-2016 model. The IMF B_Z data for these five storms have been plotted in Figure 1 to identify the PPEFs associated with the southward turning of IMF B_Z. For the March 2012 storm, no noticeable change in f_oF_2 at low-latitude stations (DW and TV) was found, but midlatitude stations (BR and CB) showed a decrease in f_oF_2 during the main phase onset of the storm starting at 15 UT (02 LT, 16 March) on 15 March, which occurred during the local nighttime of the stations and lasted into the recovery phase for several hours in the local daytime. The nighttime decrease in f_oF_2 at midlatitudes could be attributed to the PPEFs enhancing normal nighttime downward $\mathbf{E} \times \mathbf{B}$ drifts for initial several hours (Huang et al., 2005), which is consistent with the southward turning of IMF $B_Z < -5$ nT (Figure 1a) during the main phase of this storm (Tsurutani et al., 2014), before DDEFs would have spread down to midlatitude ionosphere and decreased the normal daytime upward $\mathbf{E} \times \mathbf{B}$ drifts and hence the daytime F region ionization (i.e., f_oF_2). A further contribution could be due to changes in the neutral gas composition at midlatitudes due to the storm-induced equatorward winds associated with the JH at high (auroral) latitudes indicated by a large increase in AE index (Figure 2a) that may bring the high-latitude gas with depleted O/N_2 ratio to the lower latitudes. The gas with depleted O/N_2 ratio leads to a decrease in the ionospheric electron density by increasing the recombination rates. In Figure 11, we present an analysis of daily thermospheric O/N_2 data measured by the GUVI onboard the TIMED satellite to see any change in thermospheric O/N_2 composition during the storms considered in this study. Our analysis revealed an increase in the thermospheric O/N_2 ratio at equatorial and low latitudes, which in some regions extended to midlatitudes. A decrease in O/N_2 ratio occurred at high latitudes that extended toward midlatitudes and in some cases to low latitudes as
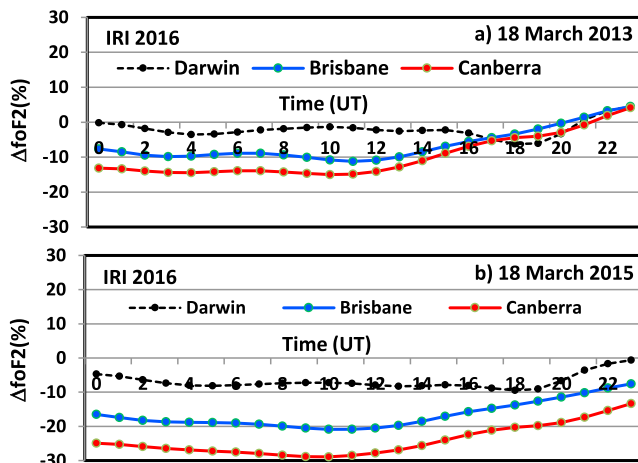

Figure 9. The percentage change in IRI-2016 given f_oF_2 on 18 March 2013 (a) and 18 March 2015 (b) for Darwin, Brisbane, and Canberra stations.
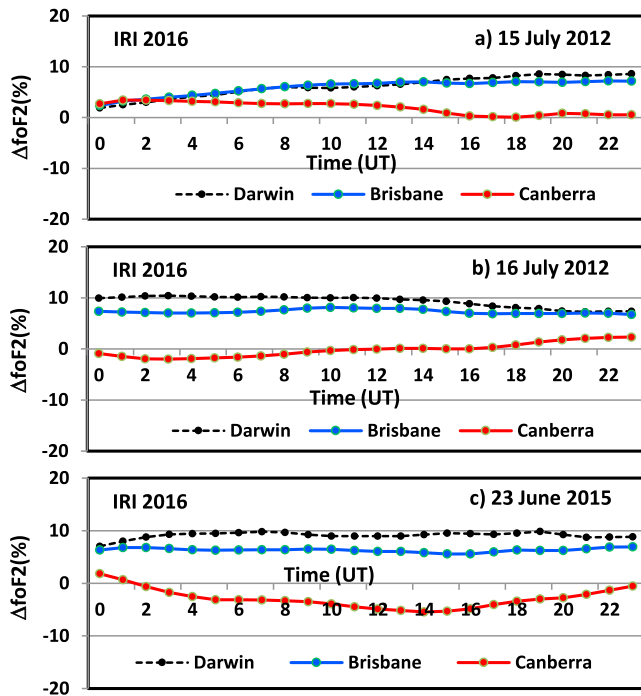
Figure 10. The percentage change in IRI 2016 given f_oF_2: (a) 15 July 2012, (b) 16 July 2012, and (c) 23 June 2015 at Darwin, Brisbane, and Canberra stations.

compared to before the storms for all five storms of this study. The changes in O/N_2 ratio started during the main phase of the storms and intensified during the recovery phases of the storms. The changes in O/N_2 ratio were most strong for the March 2015 storm followed by the March 2012, 2013, and July 2012 storms with least (or almost no change) change (increase) in O/N_2 during the June 2015 storm.

The storm-induced equatorward winds associated with the moderate strength storm of March 2012 does not seem to have propagated to the low latitudes of TV and DW stations as it is difficult for these winds to propagate to the low latitudes under the low-to-moderate strength storms (e.g., Liu et al., 2012, 2014) as can be seen by no change in thermospheric O/N_2 ratio over these stations (Figure 11a). The decrease in thermospheric O/N_2 over HO and CB stations on 16 March is consistent with the negative ionospheric effects over these two stations (Figure 2). Verkhoglyadova et al. (2014) analyzed ionospheric TEC, thermospheric cooling, column density ratio $\Sigma[O/N_2]$, and compositional changes measurements by two instruments onboard the TIMED satellite for the magnetic storm events during the 6–17 March 2012. For the 14–16 March 2012 (74 to 76 days of the year 2012), they found an increase in $\Sigma[O/N_2]$ in the daytime at low latitudes and a decrease at auroral latitudes to midlatitudes of about 40° on 15 March. For the details about parameters $\Sigma[O/N_2]$ and O/N_2 and their behavior during quiet and storm times, the reader is referred to the papers by Stephan et al. (2008) and Bums et al. (1995).

The storm events of March 2013 and 2015 were unique in the sense that they occurred on the same day (17 March) of the year and nearly at the same time (20–22 UT) and attained maximum intensity (indicated by minimum value of *Dst* index) by the two-step development in the ring current to the different levels. The first step development of ring current of the March 2013 storm was faster and stronger as compared to the March 2015 storm, whereas the second step development of the ring current for the March 2015 storm was faster and stronger. Following the first step development of the March 2013 storm, a short-time (2–5 hr) increase (positive ionospheric storm) in the f_oF_2 occurred at all stations (middle/low to middle latitudes) excluding DW at the nighttime (19–23 LT) of 17 March 2013, indicating a reduction or reversal in the normal downward $\mathbf{E} \times \mathbf{B}$ drifts (Figure 3) due to PPEFs consistent with the long-duration southward IMF $B_Z < -5$ nT (Figure 1b; Verkhoglyadova et al., 2016) prior to the increase in f_oF_2. The increase was most evident at TV (low-latitude) station as compared to other stations with no increase at further low-latitude station (DW). On 18 March 2013, there occurred a decrease in the thermospheric O/N_2 ratio over the entire Australian region (Figure 11b) associated with which a negative ionospheric storm occurred at all the stations (Figure 3). Verkhoglyadova et al. (2016), for the March 2013 storm, analyzed the vertical total electron content (vTEC) at the northern middle and low latitudes and found an increase in the afternoon vTEC (positive ionospheric storm) up to ~20 TECU during the first step development (sheath region passage) of the March 2013 storm. During the recovery phase of the March 2013 storm, they found a long-duration (>6 hr) negative ionospheric storm in both middle- and low-latitude vTEC. Our results for the southern middle and low latitudes for the March 2013 storm are consistent with the findings of Verkhoglyadova et al. (2016). However, duration of the negative ionospheric storms (Table 1) in our study is larger at midlatitudes (21–36 hr) as compared to low latitudes (15–18 hr). The degrees of negative ionospheric effect indicated by $\Delta f_oF_2\%$ (equation (1)) is higher at midlatitudes as compared to low latitudes (Table 1) due to stronger effect of storm-induced drivers of high-latitude origin (DDEFs, O/N_2 Composition, and TIDs) at the midlatitudes as compared to the low latitudes.

During the second step storm development of the March 2015 storm, 17 March showed a nighttime (21–01 LT) short-duration positive ionospheric effect in f_oF_2 at all the stations except at a low-latitude station DW. This nighttime decrease could be associated with PPEFs associated with strong and long-duration southward IMF $B_Z < -15$ nT during the second step development of the storm (Figures 4a and 1c) to
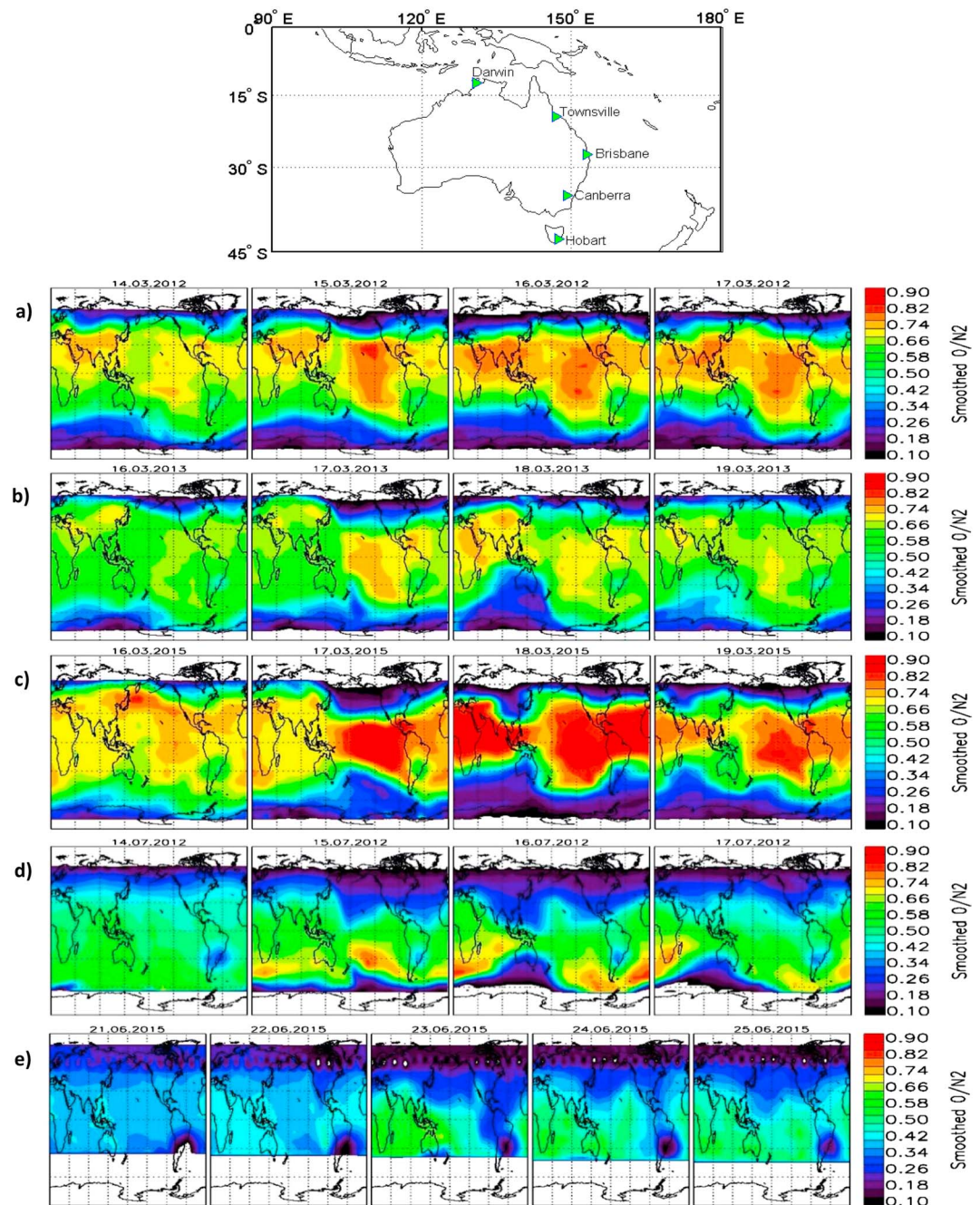
Figure 11. Daily variation of thermospheric O/N$_2$ ratio as measured by the GUVI satellite for the storms: (a) 14–17 March 2012, (b) 16–19 March 2013, (c) 16–19 March 2015, (d) 14–17 July 2012, and (e) 21–25 June 2015 globally. Data source http://guvitimed.jhuapl.edu. The locations of the stations considered in this study are shown on the map on the top of the figure.

these stations resulting in a decrease in the normal nighttime downward **E × B** drifts. The recovery phase showed a long-duration negative ionospheric effect at all the stations with Δf_oF_2% larger by about 10–15% as compared to the March 2013 storm except at HO station. During the recovery phase of this storm, there occurred a strong decrease in thermospheric O/N$_2$ density ratio over the entire Australian region (Figure 11c), which is consistent with strong negative ionospheric effect at all the stations (Figure 4). Astafyeva et al. (2015) analyzed the global ionospheric response to the March 2015 storm using multi-instrumental data recorded at northern and southern latitude stations in the

American, European-African, and Asian sectors. During the first step storm development on 17 March 2015, Astafyeva et al. (2015) observed a short-term weaker positive storm in the vTEC at low- and middle-latitude stations, and during the second step development, both the positive and negative ionospheric storms were observed at all the stations. However, during the recovery phase (within about 3 hr) on 18 March, for the Asian sector, they observed a long-duration large negative storm at high-, middle-, and at low-latitude stations. Other two sectors also showed a negative ionospheric effect but comparatively weaker and of shorter duration except at low-latitude stations in the European-African and American sectors, which first showed a moderate positive storm at the beginning of the recovery phase and then the moderate negative storm. Our results for both the March 2013 and 2015 storms are more consistent with the Asian sector results of Astafyeva et al. (2015). Astafyeva et al. (2015) also analyzed the thermospheric column integrated $\Sigma[O/N_2]$ ratio changes measured by the GUVI instrument on board TIMED satellite and found most significant $\Sigma[O/N_2]$ changes in the Asian sector (~100–130°E) and above the Australian region with decreased $\Sigma[O/N_2]$ ratio at high latitudes to midlatitudes on 18 March. As shown by our results (Figures 2–4) and the $\Delta f_oF_2\%$ calculations in the results section, the daytime (~20–08 UT) negative ionospheric effect was stronger than the nighttime (~09–19 UT). The strong reduction in the daytime f_oF_2 during the recovery phase of both March 2013 and March 2015 storms suggests that the DDEFs were westward contrary to the normal daytime eastward electric field during daytime over low and middle latitudes in Australia (Southern Hemisphere), which significantly affected the normal $\mathbf{E} \times \mathbf{B}$ drifts and reduced the ionization. Based on the analysis of the chain of ionosonde located at equatorial and low-latitude stations along with multistation GPS receivers over the Indian sector, Ramsingh et al. (2015) suggested strong signatures of DDEFs during daytime over the Indian sector associated with the March 2015 storm. They, using the ionosonde data analysis at two stations, estimated the thermospheric meridional winds and reported the TIDs associated with the gravity waves with a period of ~2 hr during the recovery phase of the March 2015 storm. Kuai et al. (2016) analyzed the ionospheric response to the March 2015 storm in the TEC and f_oF_2 over equatorial and low latitudes in the Asian-Australian and the American sectors. Over ionosonde stations at Guam (13.6°N, 144.9°E, 12.78° dip angle) and Sanya (18.3°N, 109.6°E, 24.98° dip angle) in the Asian-Australian sector, they observed negative storm effect in f_oF_2 at the nighttime during 17–18 March with the stronger and long-duration effect at Sanya station as compared to Guam. They accounted negative ionospheric effect mainly to the long-duration DDEFs in the Asian-Australian sector with effects lasting for about 1.5 days from the nighttime of 17 March to the whole day of 18 March. There have been several other studies on the topside ionospheric effects of the March 2015 storm using different techniques (e.g., Nava et al., 2016; Nayak et al., 2016; Zhong et al., 2016), showing a long-duration decrease in the topside ionization during its storm recovery phase. Some researchers (e.g., Astafyeva et al., 2015; Nava et al., 2016; Zhong et al., 2016) found significant long-lasting changes in O/N_2 at high to low latitudes during the March 2015 storm, which they accounted for the observed ionospheric effects along with the other storm-time factors. Thus, the long-duration negative ionospheric storms during the recovery phase of the March 2012, 2013, and 2015 storms, in our study, could be accounted mainly for the thermospheric O/N_2 density ratio decrease (Figures 11a–11c) due to storm-induced thermospheric winds from high latitudes with depleted O/N_2 density ratio toward lower latitudes associated with JH as indicated by large increase in AE index during the second step development of these storms (Figures 3a and 4a) and to the DDEFs particularly in the daytime. The negative ionospheric effects in high-latitude region can last for 3–4 days as long as the auroral heating due to disturbed solar winds persists, whereas in the other regions, it depends on how gas with depleted O/N_2 escapes into those regions (Kumar & Parkinson, 2017). The short-duration positive ionospheric storm in the local premidnight (March 2013 and 2015) is accounted to the PPEFs that seems to be in the opposite direction to the ambient zonal electric field reducing normal downward $\mathbf{E} \times \mathbf{B}$ drifts. Huang et al. (2016) for the March 2015 storm reported that DDEFs occurred within few hours of its main phase and lasted well into the storm recovery phase for about 31 hr. At the beginning of the March 2013 storm at 06 UT (~15–16 LT) and the March 2015 storm at 04:45UT (14–15 LT) on 17 March, the Australian sector was in the dayside, and weaker and short-duration perturbation in f_oF_2 during the main phase of these storms (Figures 2 and 3) is consistent with simulation results of Fuller-Rowell et al. (1994), which showed that the sector on the dayside at the time of beginning of the

storm is less affected as compared to the sector in the nightside. A short-duration positive ionospheric effect on 17 March of March 2013 and 2015 storms during their main phase is also consistent with findings of Jiang et al. (2017) for the March 2015 storm at low-latitude stations in the Southeast Asian region. Jiang et al. (2017) accounted short duration of ionospheric positive effect to short-term penetration of eastward and equatorward PPEFs and TADs/TIDs.

Both the March 2013 (equinoctial) storm ($Dst = -132$ nT) and the July 2012 (southern winter) storm ($Dst = -139$ nT) started in the local daytime (15–17 hr LT) of the stations, and the minimum of Dst during the first step storm development occurred in the local daytime (afternoon) and the second step storm development occurred in the postmidnight. The DW station showed a strong positive ionospheric effect during both the first and second step storm developments for the July 2012 storm with no effect during the recovery phase, whereas very contrasting effect was observed for the March 2013 storm showing no effect during both the first and second step developments and a short-duration negative ionospheric effect during the recovery phase. Other two stations (BR and CB) have shown an almost the same effect for both the storms including a long-duration (>21 hr) decrease in f_oF_2 during their recovery phases. The July 2012 storm was unique in the sense that it had the longest-duration (~31 hr) strong (< −15 nT) southward IMF B_Z (Figure 1d), which indicates that PPEFs associated with this storm were strong enough to penetrate up to low latitude of DW station. A long-duration of high AE index (Figure 5a) during the July storm, extending well into recovery phase, indicates a strong high-latitude JH to drive the storm-induced thermospheric winds to low-latitude and the gravity waves generating TADs/TIDs. A linear relationship has been reported between JH and AE index as JH = 0.19 AE (Ahn et al., 1983) and JH = 0.33 AE (Baumjohann & Kamide, 1984), where JH is in gigawatts and AE in nanotesla. The auroral activity is also indicated by the polar cap index of which data are available for March 2012, 2013, and July 2012 storms. The values of the linear correlation coefficient calculated between AE and polar cap indices for storm onset day and a day following the onset day for the March 2012, 2013, and July 2012 storms are 0.8249, 0.8864, and 0.8659, respectively. Liu et al. (2014) analyzed the ionospheric and thermospheric responses to the 15–16 July 2012 storm in the east Asian/Australian and the American sectors taking five stations from the Australian sector (including DW and BR stations) and found f_oF_2 enhancements between 01 to 10 UT on 15 July over all the five sites followed by the long-duration depressions in f_oF_2, which they accounted for neutral composition changes and DDEFs effects. Kuai et al. (2017), taking same five stations from Australia, studied the differences in the ionospheric response of the 15–16 July 2012 geomagnetic storm in the Asian-Australian (17 stations) and the American sectors. For the negative ionospheric storm in the Asian-Australian sector, they suggested a greater contribution of DDEFs than the thermospheric neutral composition changes. For the July 2012 storm, our analysis shows a decrease in thermospheric O/N_2 ratio over CB and BR stations (Figure 11d) on 16 July, which is consistent with the decrease in f_oF_2 over these two stations (Figures 5c and 5d). There was no change in f_oF_2 (Figure 5b) and no change in thermospheric O/N_2 ratio (Figure 11d) over the DW station.

The March 2015 storm ($Dst = -222$ nT) started at ~5 UT (14–15 LT) in the local daytime of the stations (Figure 3), and the minimum of Dst in the first step storm development occurred in the local evening/premidnight and in the second step storm development a minimum of Dst occurred in the local daytime (morning). The Southern Hemisphere winter storm of June 2015 ($Dst = -195$ nT) started at about 18 UT (03–04 LT) in the local postmidnight of the stations (Figure 6a), and the minimum of Dst in the first step storm development occurred in the local postmidnight/morning period and in the second step storm development a minimum of Dst occurred in the local daytime (noontime). Both the storms have shown very contrasting ionospheric effects with the June 2015 storm showing daytime (03–07 UT or 13–17 LT) short-duration (4–6 hr) strong positive ionospheric effect near its maximum intensity, whereas the March 2015 storm showed a strong long-duration negative ionospheric effect starting during the main phase and lasting well into the recovery phase. During the June 2015 storm, a slight increase in thermospheric O/N_2 density ratio occurred at all the stations (Figure 11e), whereas during the March 2015 storm, O/N_2 density ratio was the weakest over all the stations (Figure 11c, see 18 March 2015 panel). The positive ionospheric effect due to the June 2015 storm could be accounted for eastward PPEFs indicated by the IMF B_Z changes southward from about 01:50 UT (11–12 LT) on June 23 and remaining largely negative (< −15 nT; Figure 1e) until ~06 UT (Astafyeva et al., 2016). During the June 2015 storm, a slight increase in thermospheric O/N_2 ratio

occurred at all the stations (Figure 11e). The combination of a more intense storm heating and suppressed opposing poleward background circulations during the equinoctial March 2015 storm compared to June 2015 storm could explain the observations of prolonged negative ionospheric effect. Astafyeva et al. (2016) using data from multiple instruments onboard the SWARM satellites analyzed ionospheric effects for the June 2015 storm and observed both positive and negative ionospheric effects in the vTEC and the electron density in the period 19–24 UT on 22 June at the southern low and middle latitudes. From ~3 UT on 23 June, they observed a positive storm extending until 07 UT with vTEC more than twice the quiet-time values with which our results are consistent. The difference in the effect of these four storms (two equinoctial and two southern winter storms) of our study could be due to seasonal dependences of the storm effects; their start in the local day or nighttime and the storm-associated drivers; PPEFs, DDEFs, gas with depleted O/N_2 ratio, and propagation of TADs/TIDs from high latitude to middle and low latitudes; and changing the electrodynamics and composition therein, which result in the net decrease or increase in the ionization for varying duration and amount. The dominant seasonal difference in the storm effect is due to differential heating, which during winter causes background thermospheric winds to flow poleward conflicting with the storm-induced equatorward surge of thermospheric winds. During the winter storms, the depleted O/N_2 gas either may remain trapped in the high-latitude region causing no negative ionospheric storm effect at middle and low latitudes (e.g., June 2015 storm; Figure 6) or may get weak and does not propagate to low latitudes (e.g., July 2012 storm; Figure 5b).

The IRI-2016-given f_oF_2 (Figures 7, 8, and 9) during equinoctial storms of March 2013 (Figure 7) and March 2015 (Figure 8) showed a longer-duration smooth negative ionospheric effect with a smaller magnitude (Figure 9) as compared to the ionosonde given f_oF_2 (Table 1; Figures 3 and 4) particularly at midlatitude stations (BR and CB). There was no positive ionospheric effect shown by the IRI-2016 f_oF_2 during the second step of the main phase of the storms, whereas ionosonde f_oF_2 showed a short-duration positive ionospheric effect. For the Southern Hemisphere winter storms of July 2012 and June 2015, the IRI-2016 model (Figure 10) showed a much lower percentage of increase in f_oF_2 as compared to the ionosonde-observed f_oF_2 (Figures 5 and 6). During the recovery phase of July 2012 storm on 16 July, the IRI-2016 model showed an increase in f_oF_2 (Figure 10b) given by $\Delta f_oF_2\%$ (equation (1)), whereas ionosonde-observed f_oF_2 showed a decrease in f_oF_2 (Figure 5). The plausible explanation of difference in the storm effect between the ionosonde data and the IRI-2016 model data seems the limitation of the IRI storm models (IRI-2001, 2012, 2016), which use a three-hourly A_P geomagnetic index for the description of magnetic storm effects (Bilitza et al., 2014) and give monthly average behavior of the ionosphere for given solar activity level at a given place and time. The storms studied in this study occurred during moderate solar activity with observed monthly average sunspot numbers varying between 54.5 to 86.6. A description of development of IRI models from IRI-75 to IRI-2012 has been presented by Bilitza et al. (2014) and further improvements made into the 2016 version of the IRI model by Bilitza et al. (2017). For further details about IRI models, the reader is referred to IRI models web link http://irimodel.org/. The IRI model developers are suggested to further validate the performance of the IRI model during storm conditions, in particular the ability of the model to demonstrate ionospheric sensitivity to the lotion, local-time of the onset of storm, season in which storm has occurred, storm intensity, and time since the onset of storm.

5. Summary and Conclusions

During the recovery phase of the three St. Patrick Day equinoctial geomagnetic storms (March 2012, 2013, 2015), the ionosphere at the selected three southern midlatitude stations showed a long-duration negative ionospheric storm in f_oF_2, which is consistent with strength of the storms as negative ionospheric storm was most intense for the March 2015 storm ($Dst = -222$ nT), less for the March 2013 storm ($Dst = -132$ nT), and least for the March 2012 Storm ($Dst = -87$ nT). The low-latitude stations showed negative ionospheric storm of same intensity as that at midlatitudes for the March 2015 storm, comparatively weaker and shorter-duration effect for the March 2013 storm, and no effect for the March 2012 storm (not shown), indicating that the storm induced changes/drivers of high-latitude origin (DDEFs, O/N_2 Composition, TIDs) did not penetrate to low latitudes for the March 2012 storm, got weaker as they moved from high to low latitudes for the March 2013 storm, but for the superstorm of March 2015, the ionosphere at both low and midlatitudes by these drivers was severely affected with almost the same intensity. These

findings have been summarized in Table 1. The strong- and long-duration negative ionospheric effect is mainly due to the transport of high-latitude gas with depleted O/N_2 ratio (Figure 11) and the TADs/TIDs moving to lower latitudes associated with the high-latitude JH and partly due to the effect of PPEFs and/or DDEFs. The strong decrease in the f_oF_2 (negative ionospheric effect) during the local daytime (~20–08 UT) as compared to the local nighttime (08–20 UT) for the March 2013 and 2015 storms indicates very strong daytime storm-induced equatorward winds as compared to background day-to-night winds which are both in opposite direction in the daytime. A short- (2–3 hr) duration positive ionospheric storm during the main phase of the March 2013 and 2015 storms could be accounted for PPEFs that showed clear signatures at the TV (geomag. lat. 28.95°S) and no signatures at DW (geomag. lat. 21.96°). The stronger and longer duration of negative effect of these storms at midlatitudes as compared to low latitudes could be mainly accounted for latitudinal dependence of the storm effects as these storms occurred during moderate solar activity and there is not much difference in longitude of the stations except of station DW where longitudinal effect may also be a contributory factor.

A comparison of the storm effects in ionosonde-observed f_oF_2 by the similar strength March 2013 storm with the Southern Hemisphere winter storm of July 2012 (Table 2) at low-latitude station DW during the main phase shows no change in f_oF_2 for the March 2013 storm but a strong increase in f_oF_2 for the July 2012 storm. Both the storms showed a long-duration decrease in f_oF_2 at midlatitude stations, BR and CB, which was stronger and comparatively longer for the March 2013 storm. Similarly, a comparison of the March 2015 storm effect on f_oF_2 with the similar strength Southern Hemisphere winter storm of June 2015 (Table 3) gives very contrasting ionospheric effects with the March 2015 storm producing a strong long-duration (>6 hr) negative ionospheric effect, and the June 2015 storm giving a short-duration (4–6 hr) strong positive ionospheric effect during their recovery phases. This difference is partly due to more pronounced occurrence of positive ionospheric storms due to winter storms as compared to other season storms (Fuller-Rowell et al., 1996; Kumar & Parkinson, 2017). Thus, in terms of ionospheric effects, the storms are unique, as their effects depend upon their start in the local day or nighttime, season, ionospheric electrodynamical and compositional changes, and TIDs associated with atmospheric gravity waves affecting different locations differently.

The ionospheric effect of storms (March 2013, 2015, July 2012, and June 2015) on the f_oF_2 given by IRI-2016 model are summarized in Table 4 and compared with ionosonde observations given in Tables 1–3. In general, the increase/decrease in the IRI-2016 given f_oF_2 is smaller but of longer duration as compared to the ionosonde observed f_oF_2 both for equinoctial and winter time storms. Moreover, the IRI-2016 model showed positive ionospheric effect in contrast to the negative ionosphere effect shown by ionosonde f_oF_2 data during the recovery phase of July 2012. A study of large no storms using the IRI-2016 model data and their comparison with the ionosonde data is suggested to get better insight into the IRI-2016 model for any further development to improve performance of the storm-time model, which was first introduced in the IRI-2001 model with further development made in the IRI-2012 model related to storm-time model for auroral E region (Bilitza et al., 2014).

References

Ahn, B.-H., Akasofu, S.-I., & Kamide, Y. (1983). The Joule heat production rate and the particle energy injection rate as a function of the geomagnetic indices *AE* and *AL*. *Journal of Geophysical Research*, *88*, 6275–6287.

Alberti, T., Consolini, G., Lepreti, F., Laurenza, M., Vecchio, A., & Carbone, V. (2017). Timescale separation in the solar wind-magnetosphere coupling during St. Patrick's Day storms in 2013 and 2015. *Journal of Geophysical Research: Space Physics*, *122*, 4266–4283. https://doi.org/10.1002/2016JA023175

Astafyeva, E., Zakharenkova, I., & Alken, P. (2016). Prompt penetration electric fields and the extreme topside ionospheric response to the June 22–23, 2015 geomagnetic storm as seen by the Swarm constellation. *Earth, Planets and Space*, *68*(1), 152. https://doi.org/10.1186/s40623-016-0526-x

Astafyeva, E., Zakharenkova, I., & Förster, M. (2015). Ionospheric response to the 2015 St. Patrick's Day storm: A global multi-instrumental overview. *Journal of Geophysical Research: Space Physics*, *120*, 9023–9037. https://doi.org/10.1002/2015JA021629

Baker, D. N., Jaynes, A. N., Li, X., Henderson, M. G., Kanekal, S. G., Reeves, G. D., et al. (2014). Gradual diffusion and punctuated phase space density enhancements of highly relativistic electrons: Van Allen Probes observations. *Geophysical Research Letters*, *41*, 1351–1358. https://doi.org/10.1002/2013GL058942

Balan, N., Yamamoto, M., Liu, J. Y., Liu, H., & Lühr, H. (2011). New aspects of thermospheric and ionospheric storms revealed by CHAMP. *Journal of Geophysical Research*, *116*, A07305. https://doi.org/10.1029/2010JA016399

Baumjohann, W., & Kamide, Y. (1984). Hemispherical Joule heating and the *AE* indices. *Journal of Geophysical Research*, *89*, 383–388. https://doi.org/10.1029/JA089iA01p00383

Bilitza, D., Altadill, D., Truhlik, V., Shubin, V., Galkin, I., Reinisch, B., & Huang, X. (2017). International Reference Ionosphere 2016: From ionospheric climate to real-time weather predictions. *Space Weather*, *15*, 418–429. https://doi.org/10.1002/2016SW001593

Bilitza, D., Altadill, D., Zhang, Y., Mertens, C., Truhlik, V., Richards, P., et al. (2014). The International Reference Ionosphere 2012—A model of international collaboration. *Journal of Space Weather and Space Climate*, *4*, 1–12. https://doi.org/10.1051/swsc/2014004

Blanc, M., & Richmond, A. D. (1980). The ionospheric disturbance dynamo. *Journal of Geophysical Research*, *85*, 1669–1686. https://doi.org/10.1029/JA085iA04p01669

Bums, A. G., Killeen, T. L., Deng, W., & Carignan, G. R. (1995). Geomagnetic storm effects in the low- to middle-latitude upper thermosphere. *Journal of Geophysical Research*, *100*, 14,673–14,691. https://doi.org/10.1029/94JA03232

Fejer, B. G. (2011). Low latitude ionospheric electrodynamics. *Space Science Reviews*, *158*(1), 145–166. https://doi.org/10.1007/s11214-010-9690-7

Fejer, B. G., Larsen, M. F., & Farley, D. T. (1983). Equatorial disturbance dynamo electric fields. *Geophysical Research Letters*, *10*, 537–540. https://doi.org/10.1029/GL010i007p00537

Fuller-Rowell, T. J., Codrescu, M. V., Moffett, R. J., & Quegan, S. (1994). Response of the thermosphere and ionosphere to geomagnetic storms. *Journal of Geophysical Research*, *99*, 3893–3914. https://doi.org/10.1029/93JA02015

Fuller-Rowell, T. J., Codrescu, M. V., Rishbeth, H., Moffett, R. J., & Quegan, S. (1996). On the seasonal response of the thermosphere and ionosphere to geomagnetic storms. *Journal of Geophysical Research*, *101*, 2343–2353. https://doi.org/10.1029/95JA01614

Gonzalez, W. D., Joselyn, J. A., Kamide, Y., Kroehl, H. W., Rostoker, G., Tsurutani, B. T., & Vasyliunas, V. M. (1994). What is a geomagnetic storm? *Journal of Geophysical Research*, *99*, 5771. https://doi.org/10.1029/93JA02867

Gonzalez, W. D., & Tsurutani, B. T. (1987). Criteria of interplanetary parameters causing intense magnetic storms. *Planetary and Space Science*, *35*(9), 1101–1109. https://doi.org/10.1016/0032-0633(87)90015-8

Guerrero, A., Palacios, J., Rodríguez-Bouza, M., Rodríguez-Bilbao, I., Aran, A., Cid, C., & Cerrato, Y. (2017). Storm and substorm causes and effects at midlatitude location for the St. Patrick's 2013 and 2015 events. *Journal of Geophysical Research: Space Physics*, *122*, 9994–10,011. https://doi.org/10.1002/2017JA024224

Habarulema, J. B., Katamzi, Z. T., & Yizengaw, E. (2015). First observations of poleward large-scale traveling ionospheric disturbances over the African sector during geomagnetic storm conditions. *Journal of Geophysical Research: Space Physics*, *120*, 6914–6929. https://doi.org/10.1002/2015JA021066

Huang, C.-S. (2008). Continuous penetration of the interplanetary electric field to the equatorial ionosphere over eight hours during intense geomagnetic storms. *Journal of Geophysical Research*, *113*, A11305. https://doi.org/10.1029/2008JA013588

Huang, C.-S., Foster, J. C., & Kelley, M. C. (2005). Long-duration penetration of the interplanetary electric field to the low-latitude ionosphere during the main phase of magnetic storms. *Journal of Geophysical Research*, *110*, A11309. https://doi.org/10.1029/2005JA011202

Huang, C.-S., Wilson, G. R., Hairston, M. R., Zhang, Y., Wang, W., & Liu, J. (2016). Equatorial ionospheric plasma drifts and O^+ concentration enhancements associated with disturbance dynamo during the 2015 St. Patrick's Day magnetic storm. *Journal of Geophysical Research: Space Physics*, *121*, 7961–7973. https://doi.org/10.1002/2016JA023072

Jiang, C., Yang, G., Liu, J., Yokoyama, T., Liu, T., Lan, T., et al. (2017). Equatorial and low-latitude ionospheric response to the 17–18 March 2015 great storm over Southeast Asia longitude sector. *Journal of Geophysical Research: Space Physics*, *122*, 5756–5767. https://doi.org/10.1002/2017JA024134

Kuai, J., Liu, L., Lei, J., Liu, J., Zhao, B., Chen, Y., et al. (2017). Regional differences of the ionospheric response to the July 2012 geomagnetic storm. *Journal of Geophysical Research: Space Physics*, *122*, 4654–4668. https://doi.org/10.1002/2016JA023844

Kuai, J., Liu, L., Liu, J., Sripathi, S., Zhao, B., Chen, Y., et al. (2016). Effects of disturbed electric fields in the low latitude and equatorial ionosphere during the 2015 St. Patrick's Day storm. *Journal of Geophysical Research: Space Physics*, *121*, 9111–9126. https://doi.org/10.1002/2016JA022832

Kumar, S. (2005). F_2-region response to geomagnetic storms at the equatorial anomaly during 1989–2001. *Physica Scripta*, *72*(1), 100–104. https://doi.org/10.1238/Physica.Regular.072a00100

Kumar, V. V., & Parkinson, M. L. (2017). A global scale picture of ionospheric peak electron density changes during geomagnetic storms. *Space Weather*, *15*, 637–652. https://doi.org/10.1002/2016SW001573

Liu, J., Liu, L., Nakamura, T., Zhao, B., Ning, B., & Yoshikawa, A. (2014). A case study of ionospheric storm effects during long-lasting southward IMF B_z-driven geomagnetic storm. *Journal of Geophysical Research: Space Physics*, *119*, 7716–7731. https://doi.org/10.1002/2014JA020273

Liu, J., Liu, L., Zhao, B., Wei, Y., Hu, L., & Xiong, B. (2012). High-speed stream impacts on the equatorial ionization anomaly region during the deep solar minimum year 2008. *Journal of Geophysical Research*, *117*, A10304. https://doi.org/10.1029/2012JA018015

Lyons, L. R., Gallardo-Lacourt, B., Zou, S., Weygand, J. M., Nishimura, Y., Li, W., et al. (2016). The 17 March 2013 storm: Synergy of observations related to electric field modes and their ionospheric and magnetospheric effects. *Journal of Geophysical Research: Space Physics*, *121*, 10,880–10,897. https://doi.org/10.1002/2016JA023237

Marubashi, K., Cho, K. S., Kim, R. S., Kim, S., Park, S.-H., & Ishibashi, H. (2016). The 17 March 2015 storm: The associated magnetic flux rope structure and the storm development. *Earth, Planets and Space*, *68*(1), 173–184. https://doi.org/10.1186/s40623-016-0551-9

Mendillo, M. (2006). Storms in the ionosphere: Patterns and processes for total electron content. *Reviews of Geophysics*, *144*, RG4001. https://doi.org/10.1029/2005RG000193

Nava, B., Rodríguez-Zuluaga, J., Alazo- Cuartas, K., Kashcheyev, A., Migoya-Orué, Y., Radicella, S. M., et al. (2016). Middle- and low-latitude ionosphere response to 2015 St. Patrick's Day geomagnetic storm. *Journal of Geophysical Research: Space Physics*, *121*, 3421–3438. https://doi.org/10.1002/2015JA022299

Nayak, C., Tsai, L.-C., Su, S.-Y., Galkin, I. A., Tan, A. T. K., Nofri, E., & Jamjareegulgarn, P. (2016). Peculiar features of the low-latitude and midlatitude ionospheric response to the St. Patrick's Day geomagnetic storm of 17 March 2015. *Journal of Geophysical Research: Space Physics*, *121*, 7941–7960. https://doi.org/10.1002/2016JA022489

Prasad, R., Kumar, S., & Jayachandran, P. T. (2016). Receiver DCB estimation and GPS vTEC study at a low latitude station in the South Pacific. *Journal of Atmospheric and Solar - Terrestrial Physics*, *149*, 120–130. https://doi.org/10.1016/j.jastp.2016.10.004

Ramsingh, S., Sripathi, S., Sreekumar, S., Banola, K., Emperumal, P. T., & Kumar, B. S. (2015). Low-latitude ionosphere response to super geomagnetic storm of 17/18 March 2015: Results from a chain of ground based observations over Indian sector. *Journal of Geophysical Research: Space Physics*, *120*, 10,864–10,882. https://doi.org/10.1002/2015JA021509

Ray, S., Roy, B., Paul, K. S., Goswami, S., Oikonomou, C., Haralambous, H., et al. (2017). Study of the effect of 17–18 March 2015 geomagnetic storm on the Indian longitudes using GPS and C/NOFS. *Journal of Geophysical Research: Space Physics*, *122*, 2551–2563. https://doi.org/10.1002/2016JA023127

Scherliess, L., & Fejer, B. G. (1997). Storm time dependence of equatorial disturbance dynamo zonal electric fields. *Journal of Geophysical Research*, *102*, 24,037–24,046. https://doi.org/10.1029/97JA02165

Stephan, A. W., Meier, R. R., & Paxton, L. J. (2008). Comparison of global ultraviolet Imager limb and disk observations of column O/N_2 during a geomagnetic storm. *Journal of Geophysical Research*, *113*, A01301. https://doi.org/10.1029/2007JA012599

Titheridge, J. E., & Buonsanto, M. J. (1988). A comparison of Northern and Southern Hemisphere TEC storm behavior. *Journal of Atmospheric and Terrestrial Physics*, *50*, 763–780.

Tsurutani, B. T., Echer, E., Shibata, K., Verkhoglyadova, O. P., Mannucci, A. J., Gonzalez, W. D., et al. (2014). The interplanetary causes of geomagnetic activity during the 7–17 March 2012 interval: A CAWSES II overview. *Journal of Space Weather and Space Climate*, *4*, A02. https://doi.org/10.1051/swsc/2013056

Verkhoglyadova, O. P., Tsurutani, B. T., Mannucci, A. J., Mlynczak, M. G., Hunt, L. A., & Paxton, L. J. (2014). Ionospheric TEC, thermospheric cooling and O/N_2 compositional changes during the 6–17 March 2012 magnetic storm interval (CAWSES II). *Journal of Atmospheric and Solar-Terrestrial Physics*, *115-116*, 41–51. https://doi.org/10.1016/j.jastp.2013.11.009

Verkhoglyadova, O. P., Tsurutani, B. T., Mannucci, A. J., Mlynczak, M. G., Hunt, L. A., Paxton, L. J., & Komjathy, A. (2016). Solar wind driving of ionosphere-thermosphere responses in three storms near St. Patrick's Day in 2012, 2013, and 2015. *Journal of Geophysical Research: Space Physics*, *121*, 8900–8923. https://doi.org/10.1002/2016JA022883

Wu, C.-C., Liou, K., Lepping, R. P., Hutting, L., Plunkett, S., Howardand, R. A., & Socker, D. (2016). The first super geomagnetic storm of solar cycle 24: "The St. Patrick's day event (17 March 2015)". *Earth, Planets and Space*, *68*(1), 151–163. https://doi.org/10.1186/s40623-016-0525-y

Zhang, S.-R., Zhang, Y., Wang, W., & Verkhoglyadova, O. P. (2017). Geospace system responses to the St. Patrick's Day storms in 2013 and 2015. *Journal of Geophysical Research: Space Physics*, *122*, 6901–6906. https://doi.org/10.1002/2017JA024232

Zhong, J., Wang, W., Yue, X., Burns, A. G., Dou, X., & Lei, J. (2016). Long-duration depletion in the topside ionospheric total electron content during the recovery phase of the March 2015 strong storm. *Journal of Geophysical Research: Space Physics*, *121*, 4733–4747. https://doi.org/10.1002/2016JA022469